Journal of Cardiovascular Magnetic Resonance®, 2(2), 97–108 (2000)

ORIGINAL ARTICLES

Function

Delineation of Normal Human Left Ventricular Twist Throughout Systole by Tagged Cine Magnetic Resonance Imaging

Christine H. Lorenz,[1,2] John S. Pastorek,[3] and Jeffrey M. Bundy[2,4]

[1] *Cardiovascular Division, Barnes-Jewish Hospital, Washington University Medical Center, St. Louis, Missouri*
[2] *Departments of Radiology and Radiological Sciences and of Biomedical Engineering, Vanderbilt University, Nashville, Tennessee*
[3] *Division of Pediatric Cardiology, Vanderbilt University, Nashville, Tennessee*
[4] *Siemens Medical Systems, Iselin, New Jersey*

ABSTRACT

Myofibril shortening and the oblique fiber orientation of the left ventricular myocardium results in a twisting motion of the left ventricle. Advances in cardiac magnetic resonance imaging (MRI) have made it possible to label the myocardium noninvasively and track this motion (twist) through the cardiac cycle, but little data exist on its complete systolic time course. The purpose of this study was to delineate the normal human systolic time course of ventricular twist using tagged cine-MRI. Tagged cine-MRI was performed in 10 healthy subjects. The mean systolic twist angle relative to the short axis centroid for the 10 volunteers was calculated. Interstudy and intra- and interobserver variability were assessed. During isovolumic contraction, all ventricular twist was counterclockwise. Later in systole, the basal segments changed direction and rotated in a clockwise direction, whereas the apical segments continued counterclockwise rotation. The midpoint for rotation was 45 ± 8% of ventricular length. The mean short axis net ventricular twist (apex-base) at 80% systole was 12.6 ±1.5 degrees. The four wall segments showed heterogeneity in twist (lateral wall, 20.6 ± 1.7 degrees; anterior wall, 17.5 ± 5.1 degrees; inferior wall, 8.8 ± 4.9 degrees; septum, 3.5 ± 2.4 degrees). The anterior and lateral walls demonstrated significantly higher twist than the other walls ($p < 0.01$). Torsion increased steadily throughout systole after isovolumic contraction, whereas twist displayed rate changes. The mean interstudy and intra- and interobserver differences were less than 2.1 degrees. The close similarity in twist between subjects and the low interstudy and inter/intraobserver variation indicates that twist is a robust parameter of myocardial function. Torsion varies smoothly during systole, which may play a role in minimizing oxygen consumption. These data can serve as a baseline from which to compare alterations in regional myocardial function in disease.

Received April 27, 1999; Accepted September 6, 1999
Address correspondence to Christine H. Lorenz.

KEY WORDS: *Left ventricle; Magnetic resonance imaging; Tagging; Torsion; Twist; Ventricular function.*

INTRODUCTION

The systolic motion of the left ventricle (LV) has been described as a "twisting" motion as early as 1669 by Lower (1). The twisting of the heart in a counterclockwise direction around its long axis when viewed from the apex was further characterized as torsion by Arts et al. (2). Arts et al. (3) developed a mathematical model for LV mechanics based on the complex interrelationship of muscle fiber direction and the need for uniform distribution of stress on each muscle fiber. The work of Arts et al. supported the idea that LV torsion was based on the hypothesis that uniform stress was to be maintained on all myofibrils in the normal heart.

Carlsson and Milne (4) were one of the earliest groups to use implanted tantalum markers to study heart wall motion. Hansen and Coworkers (5–8) characterized LV twist in the human heart using invasive markers implanted in the myocardium. They described a decrease in LV net torsion as a marker of dysfunction caused by injury to the myofibrils during acute cardiac allograft rejection. Hansen et al. demonstrated that net systolic torsion was independent of the loading conditions on the heart. They further demonstrated that net LV torsion increased with an increased contractile state of the myocardium as induced by dobutamine. Their findings supported the concepts that torsion directly reflects the ability of the myofibril to contract and that LV torsion is a reliable reflection of cardiac function. However, tagging of the myocardium with implanted markers is not feasible for routine clinical use, and therefore a need exists for noninvasive methods for identifying fiducial markers within the myocardium.

The mechanics of ventricular torsion have also been characterized in mathematical modeling terms considering certain idealized geometries. Components considered include fiber architecture, compressibility, and contractility of the myocardium. Model predictions have shown good agreement with data obtained in animal and human experiments (9).

In recent years, cardiac magnetic resonance imaging (MRI) has advanced rapidly with new techniques, including myocardial tagging. Noninvasive labeling of the myocardium using MRI was introduced concurrently by two groups (10,11). Zerhouni et al. (10) used radial tag planes and their intersection with the endocardial and epicardial contours to track LV myocardial wall motion. Axel and Dougherty (11) were the first to apply tags in a grid pattern to track the deformation of the tissue elements formed by the intersecting lines of the grid. Briefly, tagging is a noninvasive analog of the implanted marker technique that permits alterations in magnetization that appear as dark bands throughout the myocardium. As the heart contracts, the tagged tissue retains its altered magnetization and appears distinctly different in signal intensity as compared with the surrounding tissue. The resulting images give the appearance of a deforming grid attached to the myocardium.

The use of tagged cine-MRI to assess systolic twist in the short axis (SA) plane provides a noninvasive method by which to measure this unique parameter of LV wall motion. However, little is known about the expected physiologic range of twist angles, the expected physiologic regional heterogeneity of twist angles, or the time course of regional twist throughout the cardiac cycle. Earlier implanted marker studies did not permit extensive regional measurements due to the limited number of markers that could be implanted. Establishment of these normative values is essential for application to the assessment of myocardial twist in various cardiac disorders. Potential uses would include assessment of myocardial wall motion and the perturbations that occur in certain disease states such as dilated, hypertrophic, and ischemic cardiomyopathy and acute cardiac allograft rejection. In addition, little MRI data exist on the temporal course of twist throughout systole because most investigators to date have only described end-systolic twist or twist at a few points in the cardiac cycle. Thus, the purpose of this work was to determine the physiologic range of values for systolic twist, the regional heterogeneity of this parameter, and its temporal characteristics.

METHODS

Image Acquisition

Ten healthy volunteers (aged 23–41 yr, five men and five women) with no prior history of heart disease or other chronic disease were recruited for this study. All volunteers were verbally screened for evidence of chronic or acute illness, including heart disease. The

study was approved by the local institutional review board and all subjects gave written informed consent.

Imaging was performed using a 1.5-T MRI scanner (Magnetom SP4000, Siemens Medical Systems, Iselin, NJ). Normal cardiac structure and wall motion were confirmed with standard cine-MRI of the heart before tagging. Mean systolic blood pressure was 123 ± 13 mm Hg, and mean diastolic blood pressure was 75 ± 9 mm Hg. To ensure that MR exams provided data that was comparable between subjects and from exam to exam, a standard protocol was followed for image acquisition (12). The exam began with a sagittal image to locate the position of the heart in the chest. A transverse image was then obtained to visualize the interventricular septum. Images parallel to the interventricular septum in the LV were then acquired, yielding a vertical long axis view. Images acquired through the long axis of this image resulted in a horizontal long axis view. From this view, the tricuspid and mitral valve planes were defined in the end-diastolic frame. An electrocardiogram (ECG)-triggered spatial modulation of magnetization-tagged gradient echo cine-sequence (TE/TR 14/42 msec, flip angle 20 degrees, grid spacing 7 mm, temporal resolution 42 msec, slice thickness 7 mm, slice gap 3 mm, scan matrix 128 × 256, image acquisition resolution 1.2 × 2.4 mm) was then used to acquire images throughout systole and early diastole in the SA plane from the valve plane to the apex of the heart (11). Approximately six to seven phases were analyzed in each subject, depending on heart rate. We have found this method of defining the SA view to be reproducible within a few degrees in each axis (12). This approach to data acquisition allows reproducible images of the heart in the SA view.

Image Analysis

Analysis software (TAGASIST) developed by the authors (13) was used to analyze the images. The end-diastolic image (the first image in the ECG-triggered sequence) served as a baseline reference, whereas grid intersection points were identified visually and marked manually in each temporal frame of the tagged cine-images. The myocardium was divided into triangular tissue elements using sets of adjacent grid intersection points as vertices. The epicardial and endocardial contours were traced manually for each temporal frame. The end-diastolic frame was identified as the first frame of the ECG-triggered sequence, and the end-systolic frame was identified as the frame with the smallest blood pool, before the reversal of ventricular twist angle during isovolumic relaxation. The epicardial boundary was used to calculate the center of mass of the LV at each time point, and the epicardial and endocardial borders together were used to exclude grid intersections falling outside the myocardium from further analysis. The center of mass at each time point was used because the heart can translate during the cardiac cycle, resulting in the center of mass moving between end-diastole and subsequent frames.

This procedure was repeated for six SA levels of the LV. The most basal level analyzed was defined as the highest level where the left atrium did not enter the imaging plane during systole. The intersection of the interventricular septum with the right ventricle (RV) were manually identified for each SA slice at end-diastole. The remaining LV wall was then automatically divided equally along its circumference into three equal portions and labeled as anterior, lateral, and inferior walls (Fig. 1). Each triangular element was then automatically assigned to its respective LV wall segment. Figure 2 shows an example from one subject, an SA image of a 7-mm slice at the midventricular level. The image on the left was obtained at end-diastole. The middle image is at end-systole. The image on the right shows an end-diastolic image with intersection points connected to form tissue triangular elements.

Twist Analysis

The centroid of each triangular element was calculated and referenced to the center of mass of the LV for each temporal frame throughout systole. A more detailed de-

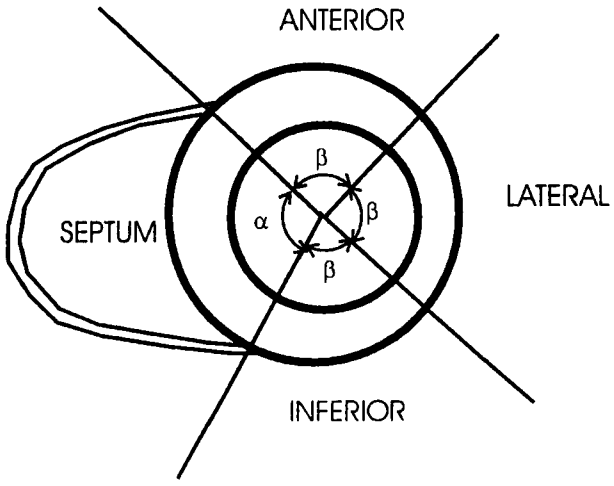

Figure 1. Segmentation of the LV SA slice into four wall segments. The septum is described by α, and the remaining free wall is divided into three equiangular sectors (β).

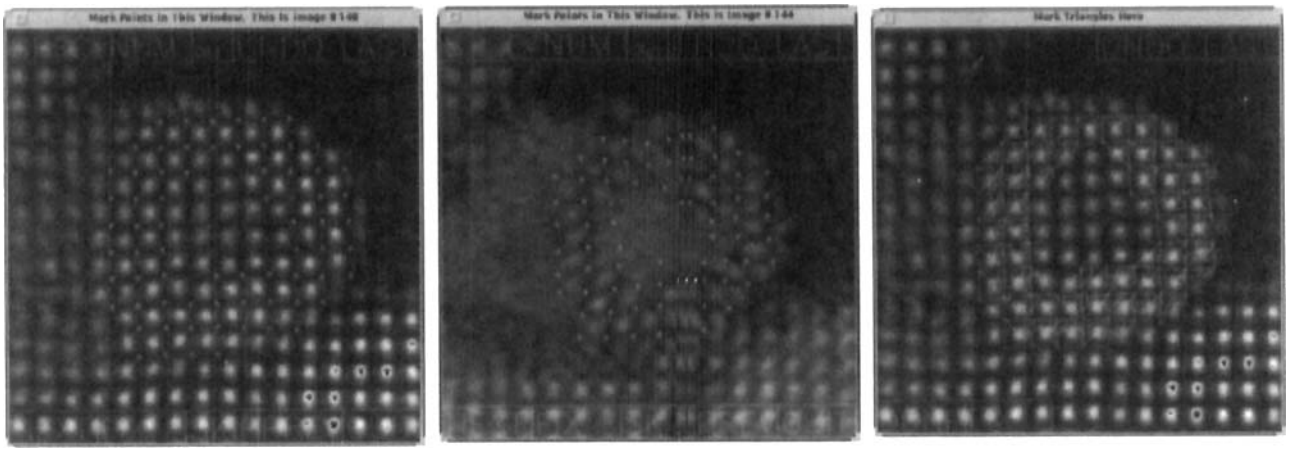

Figure 2. Demonstration at a midventricular level of identification of tag intersections at end-diastole (left) and at end-systole (middle) and demonstration of formation of triangular tissue elements (by connecting adjacent groups of three points) at end-diastole (right). The motion and deformation of the triangular elements is then tracked automatically through the remainder of the cardiac cycle using the same manually marked intersection point numbers as vertices in each subsequent frame.

scription and figures illustrating the analysis can be found in Reference 13. A number of variables have been used in the literature describing ventricular kinematics with MRI. In this study, we selected the following nomenclature and symbols. The local twist angle in slice i, $\phi_i(t)$, was defined as the angle between radial lines connecting the center of mass of the LV to the centroid of a specific triangular element at end-diastole and at any other time during systole (Fig. 3). Because the base and apex of the ventricle twist in opposite directions, we also calculate the net twist angle for the ventricle. Therefore, the net ventricular twist angle, $\phi_{net,i}(t)$, was defined as the difference between the twist angle, in any slice i, $\phi_i(t)$, and the twist angle for the corresponding area in the most basal slice, $\phi_{base}(t)$ (thus $\phi_{net,i}(t) = \phi_i(t) - \phi_{base}(t)$). The local twist angles and net ventricular twist angles for each SA slice and its four wall segments were then calculated as a function of percent systole to normalize for differences in heart rate.

The net twist angle was also expressed as a function of ventricular length to test the hypothesis that torsion, defined as twist per unit length, is constant along the length of the normal ventricle. The circumferential-longitudinal shear angle, γ_{CL}, was also computed at end-systole per wall segment as shown in Fig. 4.

Reproducibility and Statistical Analysis

The mean and standard deviation of $\phi_i(t)$ for the 10 volunteers was calculated for each slice, wall segment, and for $\phi_{net,i}(t)$. Analysis of variance for repeated measures (ANOVA) was used to test for significant differences in $\phi_i(t)$ and $\phi_{net,i}(t)$ between the four LV wall segments and the six SA levels.

To assess the variability from exam to exam of the same subject, three subjects were reimaged at 6 and 12

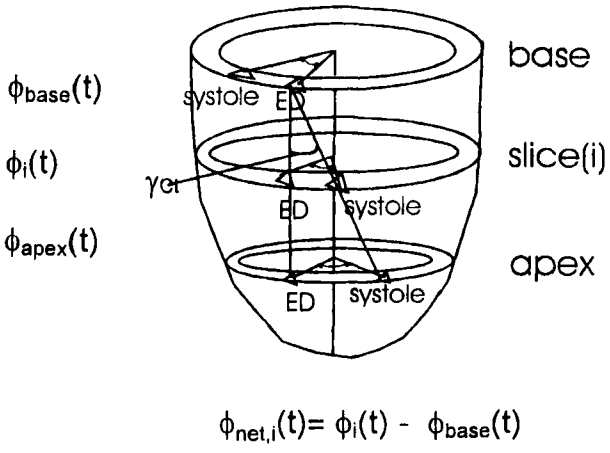

Figure 3. Definition of the twist angle of an individual triangular tissue element in an SA plane is shown ($\phi_{base}(t)$, $\phi_i(t)$, $\phi_{apex}(t)$). Also shown is the calculation of ventricular twist as the difference in twist angles between the basal slice and any other slice ($\phi_i(t) - \phi_{base}(t)$) and net ventricular twist ($\phi_{net,i}(t)$)), defined as the difference of twist angles between the most basal and any more apical slice i. The circumferential-longitudinal shear angle, γ_{CL}, is also shown.

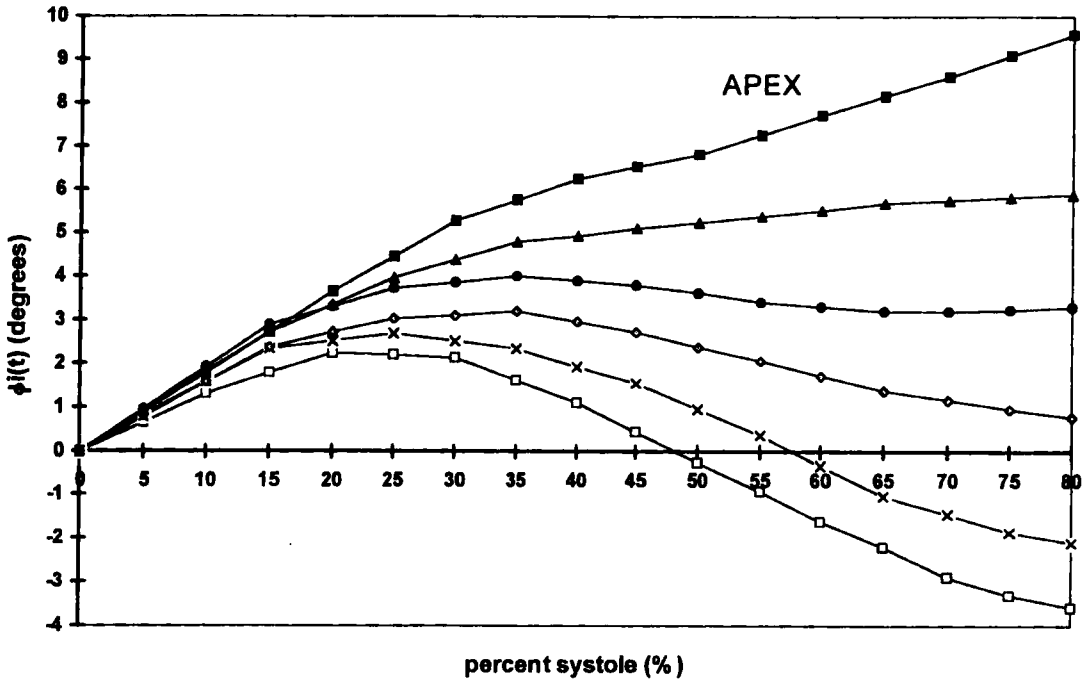

Figure 4. The average twist over each entire SA slice averaged over all 10 volunteers is shown throughout systole. The curves show a smooth transition from the monotonic counterclockwise twist at the apex (top line) to the pattern of initial counterclockwise torsion followed by clockwise torsion at the base (bottom line). Twist values were interpolated based on the original data for every 5% increment of systole. Error bars are not shown here to allow appreciation of the pattern rather than the absolute values of twist.

months. The three separate studies were analyzed by the same observer. The whole heart and regional $\phi_i(t)$ values were compared for differences using repeated measures ANOVA.

To assess the intraobserver variability, one subject's images (six SA slices labeled over seven frames in systole = 42 images) were analyzed twice by the same observer. The twist angle values averaged over the whole slice and over the four wall regions were compared for differences using repeated measures ANOVA.

To assess the interobserver variability, a single subject's images were manually labeled as described above by two observers. The whole slice and regional $\phi_i(t)$ values were compared for differences using repeated measures ANOVA.

RESULTS

Twist Pattern

The mean (averaged over all four wall segments) twist angle $\phi_i(t)$ plotted as a function of percent systole is shown in Fig. 4. The data have been interpolated to show twist at intervals of 5% systole. All six SA slices showed positive twist during the first 45% of systole. There is a transition from positive (counterclockwise) to negative (clockwise) twist in the two most basal slices between 45% and 60% of systole. The most rapid change in twist as a function of percent systole occurred within the first approximate 20% of systole for all six SA slices (Fig. 4). The rate of twist declined significantly during the last 50% of systole. This finding supports the <5% change in twist during the last 20% of systole we found in seven subjects whose data were interpretable to 100% systole as opposed to only 80% systole.

Twist

The mean and standard deviation for the local twist angle, ϕ_i, for all six SA levels and their respective LV wall segments are plotted in Fig. 5. Twist values at 80% of systole were used as opposed to those at 100% systole due to fading of tags that made analysis unreliable at end-systole in three subjects. However, in the seven subjects whose systolic twist at end-systole (100% of systole) was available, the values at 80% systole were within 5% of

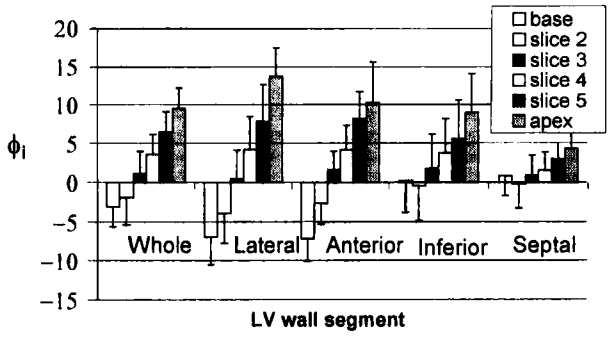

Figure 5. Mean twist angle at 80% systole for each slice position expressed as a percentage of total ventricular length (0% = base, 100% = apex). Twist is averaged over each of the four wall segments (lateral, anterior, inferior, and septal) and over the entire SA slice (whole).

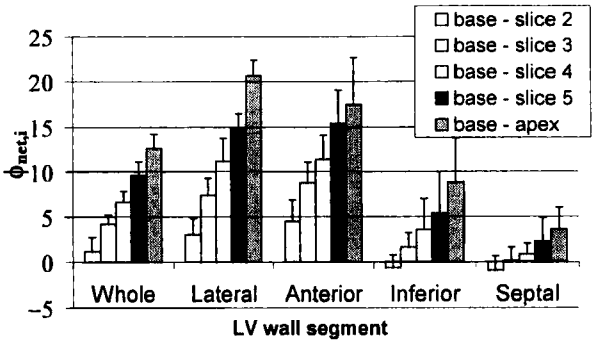

Figure 6. Ventricular twist (difference between twist at the base and any other slice *i*) between successive slices in the four wall segments and averaged over the entire slice (whole).

those at end-systole, indicating that most systolic twist had occurred by 80% systole.

The results were consistent between subjects. All 10 subjects demonstrated similar patterns of twist, with the lateral wall demonstrating the greatest net twist. The most basal slices demonstrated a characteristic early counterclockwise twist ($+\phi$) followed by clockwise twist ($-\phi$) throughout the rest of systole, whereas the apical slices consistently demonstrated a counterclockwise twist ($+\phi$). The midventricular levels demonstrated an early systolic clockwise twist, followed by end-systolic counterclockwise twist. There was a consistent transition in late systolic twist from negative to positive between 45 $\pm$ 8% of the total ventricular length in all 10 volunteers. Consistent regional differences in systolic twist were observed between the anterolateral segments and the inferoseptal segments at all SA levels ($p < 0.05$). The septal twist values were significantly smaller than each of the twist values in the other three walls ($p < 0.05$).

Net Ventricular Twist

The mean values of the net ventricular twist angle, $\phi_{net}(i)$ (at 80% systole, averaged over each wall segment), are plotted in Fig. 6. The most basal slice used in the study was obtained at 30% of total ventricular length, and all net twist calculations are thus made with respect to the twist at that basal level. The anterior and lateral walls demonstrated the greatest ventricular twist at all levels from base to apex. The septum demonstrated significantly less ventricular twist compared with the free walls ($p < 0.05$). Whole slice and lateral wall ϕ_{net} were the most consistent from subject to subject with a standard deviation of less than 1.8 degrees. Anterior and inferior wall standard deviations averaged approximately 5 degrees, and septal standard deviation averaged approximately two degrees.

Torsion and Time Course of Torsion

As can be seen in Fig. 6, there was an approximately linear relationship between the net ventricular twist angle, $\phi_{net,i}(t)$, and percent ventricular length for each wall segment and for the whole slice ($r > 0.99$), indicating that torsion, $\theta_{net,i}(t)$, is constant along the ventricular length. Table 1 summarizes these results at 80% systole. Each region of the heart (lateral, anterior, septum, inferior) had different magnitudes of θ_{net}, but each linear relationship was statistically significant. This relationship is maintained throughout systole as demonstrated in Fig. 7, where $\theta_{net}(t)$ (calculated over the entire slice and not on a regional basis) is plotted as a function of systole. All slopes were significant at the $p < 0.05$ level. In the first 20% of systole, approximately equal to the duration of the isovolumic contraction phase, all slices are moving counterclockwise as shown in Fig. 4; thus, $\theta_{net}(t)$ is approximately zero. Later in systole, there is a monotonic increase in the $\theta_{net}(i)$, indicating slowly increasing opposite motions of base and apex. Despite the decrease in rate of twist in the later half of systole, $\theta_{net}(i)$ continues to increase. This is consistent with the data in Fig. 4 that show greater divergence of base and apex and stabilization of the twist rate in the later half of systole.

Circumferential-longitudinal shear at end-systole also showed regional heterogeneity (Table 1) with the lateral

Table 1

Net Ventricular Torsion Angle as a Fraction of Ventricular Length

	Whole	Lateral	Anterior	Inferior	Septum
Slope (degrees/fraction ventricular length)	24.6	38.6	33.2	17.4	7.6
Intercept	−11.1	−18.8	−16.0	−6.3	−2.5
r	0.994	0.996	0.993	0.958	0.903
Standard error slope	1.4	1.7	1.9	2.6	1.8
Standard error intercept	0.8	1.0	1.1	1.5	1.1
p					
Slope	<0.001	<0.001	<0.001	0.003	0.01
Intercept	<0.001	<0.001	<0.001	0.01	0.08
γ (at 100% ventricular length)	7.8	11.5	9.9	6.4	2.9

and anterior walls exhibiting the largest shear angles (11.5 and 9.9 degrees, respectively) and the septum exhibiting the smallest shear angle (2.9 degrees).

Reproducibility and Observer Variability

The mean interstudy difference for $\phi_i(t)$ for all segments between the three repeated studies was 2.1 ± 1.6 degrees. There was no significant difference for all $\phi_i(t)$ measured in the three repeated studies ($p = 0.92$). The mean intraobserver difference in twist in a midventricular slice through seven separate frames of systole was less than 0.05 degrees. The mean interobserver difference for twist angle in the same slice was 0.1 ± 0.1 degrees.

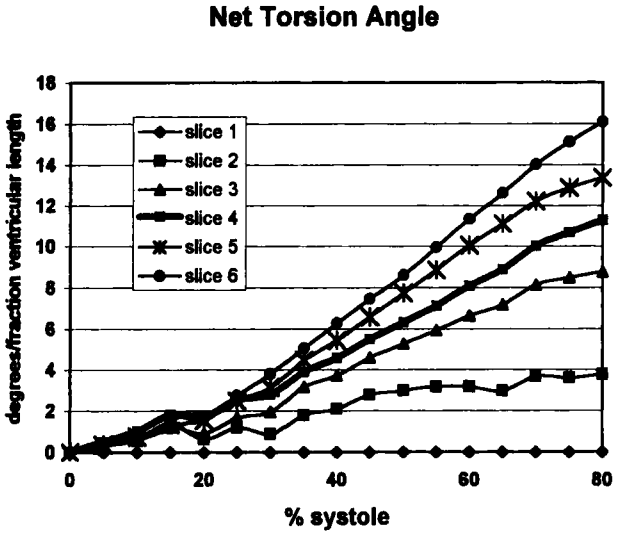

Figure 7. The net ventricular twist angle as a function of fraction ventricular length (net torsion angle) is a constant at each point in systole. During the first 20% of systole, all slices are moving in a counterclockwise direction, leading to a value of zero (ϕ_{net}/fraction ventricular length). Later in systole there is a monotonic increase in this value.

DISCUSSION

Regional Heterogeneity

Consistent regional differences in local systolic twist, $\phi_i(t)$, were observed between the anterolateral segments and the inferoseptal segments at all SA levels ($p < 0.05$). The anterior and lateral walls demonstrated the greatest net twist from base to apex. The septum demonstrated significantly less net twist as compared with the free wall segments ($p < 0.05$). This finding was consistent with that of other MRI tagging studies (14,15) and invasive marker data (5–7,16). This regional heterogeneity in twist likely reflects the known heterogeneity of fiber architecture (17). Young et al. (18), however, did not demonstrate these significant regional differences with MRI. This discrepancy may be explained in part by the differences in the calculation of the LV's center of rotation and LV wall segmentation between this study and Young's study. We also recognize that the true center of rotation for the LV may be about the center of the RV and LV combined as suggested by Young et al. (18). The true center of rotation of the LV is not yet known and awaits further study.

Anatomic studies have shown significant fiber crossover between LV and RV along the anterior interventricular sulcus and very little crossover posteriorly (17). This may provide the anterior wall greater mechanical advantage during systole as it is pulled with the RV, thus accounting for the greater twist values obtained for the ante-

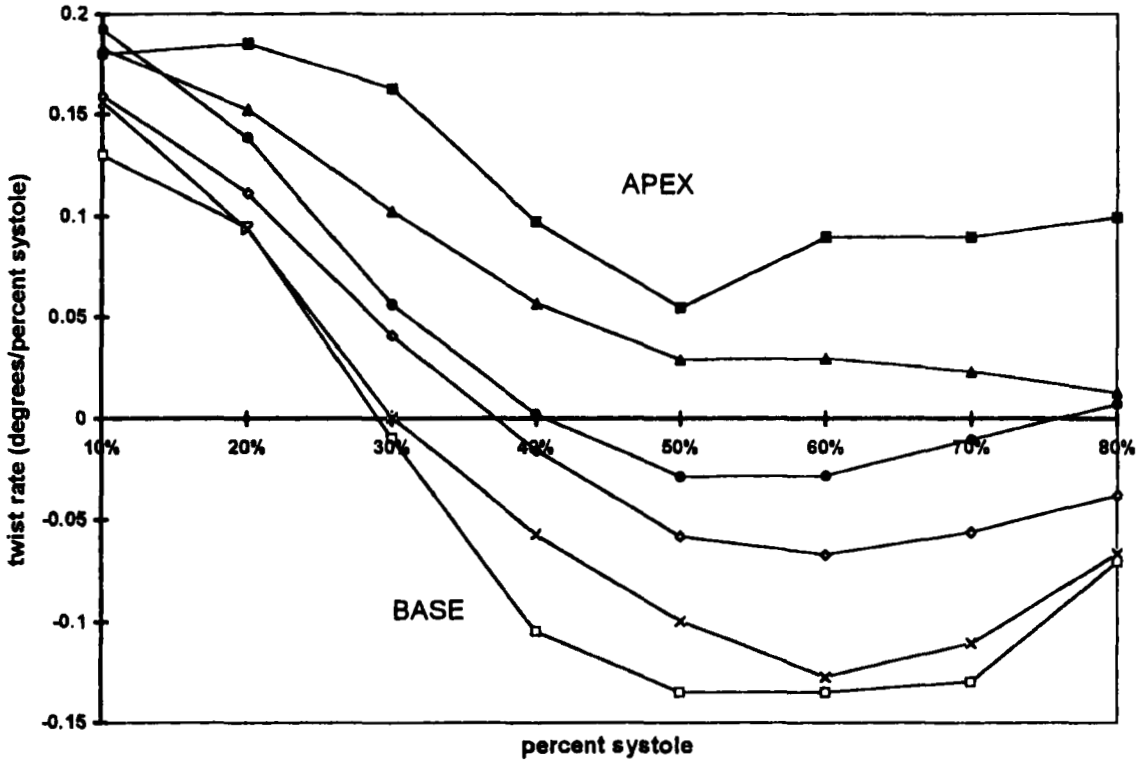

Figure 8. The rate of twist (degrees/percent systole) is shown throughout systole. Initial rapid twisting occurs in the first 20% of systole, followed by a transition to a slower more stable rate of twist in the latter 50% of systole.

rior and lateral walls. The precise role of the papillary muscles anchored in the lateral myocardial wall and their role in facilitating twist remains to be elucidated.

We recognize that isolating the two ventricles from each other makes the false assumption of no functional interactions. The consistent differences between myocardial wall segments observed within this normal group and in previous studies likely reflects the complex interrelationship of the RV and LV.

Ventricular Shear and Time Course of Torsion and Twist

The torsion angle was shown to be approximately zero through isovolumic contraction and later increasing monotonically throughout systole, supporting the theory proposed by Arts et al. (3), Buchalter et al. (14), and others that fiber shear is uniform over the heart, which may have implications for minimizing oxygen consumption. Such uniform distribution of shear is thought to be essential for optimal delivery of mechanical forces by the obliquely oriented myocardial muscle fibers (3). Although torsion increases during systole, the temporal changes are smooth, and this lack of abrupt changes (i.e., little acceleration of shear) may also minimize energy utilization.

Buchalter et al. (14) computed shear using myocardial tagging in two layers across the myocardium at end-systole and found similar values of shear transmurally, despite increased endocardial twist. The end-systolic values for circumferential-longitudinal shear angle in Buchalter's study are similar to ours (approximately 5 degrees for the entire ventricle vs. our value of 8 degrees). Arts et al. (19) found this shear value in the dog to be approximately 7 degrees using echocardiography, also consistent with our results.

The difference in shearing behavior between the isovolumic contraction period and the remainder of systole may be indicative of different mechanisms of wall contraction for generating pressure and for ejecting blood. In the isovolumic contraction period, the entire ventricle from base to apex rotates in the same direction (counterclockwise) and then begins twisting in opposite directions later in systole. In an early cineangiographic study

with implanted markers, McDonald (20) also demonstrated an early counterclockwise rotation of the ventricle in the isovolumic contraction phase. Ingels et al. (7) proposed a mechanism by which the time sequence of activation of the endo- and epicardial fibers results in twist and could explain the change in shear from early to midsystole. They propose that the early systolic twist is due to activation of the subendocardial fibers in a right-handed helix that stiffens the ventricle and begins generation of LV pressure. They hypothesize that midwall activation continues this pressure development without much contribution to twist because the fibers here are organized in the mostly circumferential direction. Later, when the subepicardial fibers are activated, they dominate twist and overtake the effect of endocardial fiber activation. This delay in activation across the wall may well explain the changing time course of twist seen in this study, but further work remains to define the exact relationship between activation and twist. Early systolic twist magnitude or rate may be related to peak dP/dt, but again, further work is required to test this hypothesis.

Rademakers et al. (21) studied the relationship between cross-fiber shortening and wall thickening using MRI myocardial tagging combined with fiber angle determinations. The components of strain along and perpendicular to the fiber orientation were determined. At the epicardium, cross-fiber strain was near zero, but at the endocardium cross-fiber strain was large and increased from base to apex. The main conclusion of their study was that the interaction between layers of the myocardium is the primary source of wall thickening. LeGrice et al. (22) showed that shear along cleavage planes in the inner third of the endocardium could account for more than 50% of systolic wall thickening. These findings are consistent with the results in this study that support the premise that shearing of the ventricle is an important contributor to wall motion.

Reproducibility

There was no significant difference for twist angle measured in the three repeated studies ($p = 0.92$). Although the tag intersection points were marked manually, the minimal inter- and intraobserver and interstudy variability supports tagged cine-MRI as a reliable and reproducible means of assessing systolic twist of the LV noninvasively. It appears that twist, similar to other functional parameters (i.e., shortening fraction, ejection fraction, wall stress), is relatively constant in the resting state for healthy individuals over time. This reproducibility will prove useful for assessment of myocardial function in serial studies of the same subject. These data should also serve as a baseline from which to compare alterations in myocardial function in other patient populations.

Study Limitations

Limitations include the temporal and spatial resolution attainable in this study. Systolic twist could be reliably measured through 80% of systole in all subjects and through 100% systole in seven subjects. The tag spacing in this study was limited to a 7 × 7-mm grid. This allowed only two to three triangular elements labeled between endocardial and epicardial surface in the normal adult LV and would be even more limited in the pediatric population and dilated cardiomyopathy population due to smaller wall thickness. However, recent advances in tagging techniques and improved imaging hardware will minimize the effects of tag fading and reduce the tag spacing interval to overcome these limitations (23–27). Some investigators have divided the myocardium transmurally into epicardial and endocardial segments to study deformation parameters across the wall. We did not have that capability for this study.

A further limitation of the technique used in this study is that it cannot take through-plane motion into account. Motion of the myocardium through-plane is greatest at the base of the heart, and errors due to this motion can be expected to be greatest there. However, newer techniques that allow tracking of the same slice of tissue throughout the cardiac cycle (24) will help to overcome this problem and allow determination of the magnitude of error resulting from non-slice following techniques. Further, methods that allow calculation of three-dimensional deformation from orthogonal sets of tagged images (long axis and SA) (28,29) will also serve to reduce errors due to through-plane myocardial motion. Comparisons between studies taking this motion into account and those that do not therefore should be interpreted carefully, especially at the base of the ventricle.

The labor-intensive off-line analysis of the tagged cine-MR images continues to be a limiting factor for routine clinical evaluation of tagged cine-MRI. However, technical advancements are being made to create usable software for handling the large amount of data created by the tagging technique and to automate the labeling and analysis of the images (28,30,31).

Image acquisition times could also be reduced to broaden the application of this technique. At the time of this study, total acquisition times for this protocol ranged between 30 and 45 min, including scout views for de-

termining the SA plane. Ongoing work, including development of breathhold tagging sequences, will shorten this examination time to a reasonable length for using tagging as an "add-on" to the rest of a cardiac MR exam.

Clinical Implications

The time course and the magnitude of ventricular twist may have clinical implications, especially in those disorders where fiber orientation or myocardial stiffness are altered. In ventricular remodeling after infarction, where the extracellular matrix is changing in both composition and material properties, the mechanisms of wall thickening, even in remote regions of myocardium, may be altered as a compensatory measure. Kramer et al. (32) recently showed that strain parameters calculated from tagged cine-MRI are altered in infarcted and remote myocardial regions and that angiotensin-converting enzyme inhibitors can retard this effect. Sayad et al. (33) demonstrated that segmental contractile reserve can predict improvement in end-systolic wall thickness after revascularization. Ventricular twist in addition to strain is also altered in remodeling and is a parameter that potentially integrates the net effect of changing myocardial strain (34).

Ventricular twist has also been shown to be altered in hypertrophic cardiomyopathy. Young et al. (35) found a reduction in shortening in the septum but overall greater net twist at end-systole (19.9 vs. 14.6 degrees, $p < 0.01$). Pastorek et al. (36) also found similar results with increased end-systolic twist in hypertrophic cardiomyopathy as compared with normal (19.1 vs. 12.6 degrees, $p < 0.01$). The dynamics of twist have been shown to be altered in hypertrophic cardiomyopathy (37,38) with the early rapid twisting in early systole and the rapid untwisting in early diastole (39) prolonged throughout systole and diastole. This finding is consistent with the known findings of decreased shortening velocity and delayed relaxation in these patients. In comparison, a control group of elite athletes with matched cardiac hypertrophy showed normal rapid twisting and untwisting. These results may lead to ways to differentiate physiologic from pathologic hypertrophy and to study the effects of fiber disarray in hypertrophic cardiomyopathy. Buchalter et al. (40) demonstrated in dogs that regional torsion in remote areas is affected by abnormal torsion in focal areas (e.g., due to ischemia or pacing), demonstrating the effects of the complex fiber arrangement in the ventricle. Based on a computer model, Beyar and Sideman (41) proposed that alterations in torsion in hypertrophic cardiomyopathy may alter the gradient of sarcomere work across the wall and thus increase oxygen utilization, leading to subendocardial fibrosis. This speculation remains to be proven in vivo, however.

As discussed in the Introduction, Hansen et al. (6) demonstrated with implanted markers that torsion may be a relatively load independent measure of contractile function with end-systolic twist increasing with inotropic stimulation. However, MacGowan et al. (42) showed that torsion is afterload dependent in the isolated dog heart. More work is needed to determine whether there is a role for using torsion or torsion-volume loops as a measure of contractile function or for diastolic function assessment.

SUMMARY

Despite regional heterogeneity in twist, twist integrated over each slice is smoothly varying through the cardiac cycle, reflecting the role of the complex fiber arrangement in the LV. In the normal ventricle, circumferential-longitudinal shear also shows regional heterogeneity. There are three distinct phases of twist. During the isovolumic contraction period, twist is uniformly counterclockwise from base to apex, and twist rate is high. In mid-systole, twist is decelerating, and in the remainder of systole, the apex and base twist in opposite directions and twist rate becomes constant. The integrated smooth torsion as a result of the fiber arrangement may have implications for minimizing oxygen consumption. Conversely, disruptions in torsion due to fiber disarray or infarction, for example, may affect ventricular performance and remodeling. Further work is necessary to determine the specific effects of local torsion disruption on global torsion and ventricular function.

ACKNOWLEDGMENT

We thank Drs. Stefan Fischer and Samuel Wickline for helpful comments on the manuscript.

REFERENCES

1. Lower R. Tracus de Corde. 1669. In: Gunther RT, ed. *Early Science in Oxford.* Vol. 9. Oxford, UK: 1932. Reprint. London: Sawsons, Pall Mall, 1968.
2. Arts T, Veenstra PC and Reneman RS. Epicardial deformation and left ventricular wall mechanics during ejection in the dog. *Am J Physiol*, 1982; 243:H379–H390.
3. Arts T, Reneman RS and Veenstra VC. A model of the mechanics of the left ventricle. *Ann Biomed Eng*, 1979; 7:299–318.

4. Carlsson E and Milne ENC. Permanent implantation of endocardial tantalum screws: a new technique for functional studies of the heart in experimental animals. *J Can Assoc Radiol*, 1967; 19:304–309.
5. Hansen DE, Daughters GT, Alderman EL, Stinson EB, Baldwin JC and Miller DC. Effect of acute cardiac allograft rejection on left ventricular systolic torsion and diastolic recoil measured by intramyocardial markers. *Circulation*, 1987; 76:988–1008.
6. Hansen DE, Daughters GT, Alderman EL, Ingels NB, Stinson EB and Miller DC. Effect of volume loading, pressure loading, and inotropic stimulation on left ventricular torsion in humans. *Circulation*, 1991; 83:1315–1326.
7. Ingels NB, Hansen DE, Daughters GT, Stinson EB, Alderman EL and Miller DC. Relation between longitudinal, circumferential, and oblique shortening and torsional deformation in the left ventricle of the transplanted human heart. *Circ Res*, 1989; 64:915–927.
8. Hansen DE, Daughters GT, Alderman EL, Ingels NB and Miller DC. Torsional deformation of the left ventricular midwall in human hearts with intramyocardial markers: regional heterogeneity and sensitivity to the inotropic effects of abrupt rate changes. *Circ Res*, 1988; 62:941–952.
9. Taber LA, Yang M and Podszus WW. Mechanics of ventricular torsion. *J Biomech*, 1996; 29:745–752.
10. Zerhouni EA, Parish DM, Rogers WJ, Yang A and Shapiro EP. Human heart: tagging with MR imaging—a method for noninvasive assessment of myocardial motion. *Radiology*, 1988; 168:59–63.
11. Axel L and Dougherty L. Heart wall motion: improved method of spatial modulation of magnetization for MR imaging. *Radiology*, 1989; 172:349–350.
12. Lorenz CH, Walker ES, Morgan VL, Klein SS and Graham TP. Normal human right and left ventricular mass, systolic function and gender differences by cine magnetic resonance imaging. *J Cardiovasc Magn Reson*, 1999; 1: 7–22.
13. Bundy JM, Lorenz CH. TAGASIST: a post-processing and analysis tools package for tagged magnetic resonance imaging. *Comput Med Imag Graph*, 1997; 21:225–232.
14. Buchalter MB, Weiss JL, Rogers WJ, Zerhouni EA, Weisfeldt ML, Beyar R and Shapiro EP. Noninvasive quantification of left ventricular rotational deformation in normal humans using magnetic resonance imaging myocardial tagging. *Circulation*, 1990; 81:1236–1244.
15. Maier SE, Fischer SE, McKinnon GC, Hess OM, Krayenbuehl HP and Boesiger P. Acquisition and evaluation of tagged magnetic resonance images of the human left ventricle. *Comput Med Imag Graph*, 1992; 16:73–80.
16. Beyar R, Yin FCP, Hausknecht M, Weisfeldt ML and Kass DA. Dependence of left ventricular twist-radial shortening relations on cardiac cycle phase. *Am J Physiol*, 1989; 57:H1119–H1126.
17. Greenbaum RA, Ho SY, Gibson DG, Becker AE and Anderson RH. Left ventricular fiber architecture in man. *Br Heart J*, 1981; 45:248–263.
18. Young AA, Imai H, Chang CN and Axel L. Two-dimensional left ventricular deformation during systole using magnetic resonance imaging with spatial modulation of magnetization. *Circulation*, 1994; 89:740–752.
19. Arts T, Meerbaum S, Reneman RS and Corday E. Shear of the left ventricle during the ejection phase in the intact dog. *Cardiovasc Res*, 1984; 18:183–193.
20. McDonald IG. The shape and movements of the human left ventricle during systole. *Am J Cardiol*, 1970; 26:221–230.
21. Rademakers FE, Rogers WJ, Guier WH, Hutchins GM, Siu CO, Weisfeldt ML, Weiss JL and Shapiro EP. Relation of regional cross-fiber shortening to wall thickening in the intact heart: three-dimensional strain analysis by NMR tagging. *Circulation*, 1994; 89:1174–1182.
22. LeGrice IJ, Takayama Y and Covell JW. Transverse shear along myocardial cleavage planes provides a mechanism for normal systolic wall thickening. *Circ Res*, 1995; 77:182–193.
23. Fischer SE, Stuber M, Scheidegger MB and Boesiger P. Towards high resolution myocardial tagging [abstract]. *Proc Soc Magn Reson Med*, 1993; 3:1225.
24. Fischer SE, McKinnon GC, Scheidegger MB, Prins W, Meier D and Boesiger P. True myocardial motion tracking. *Magn Reson Med*, 1994; 31:401–413.
25. O'Dell WG, Schoeniger JS, Blackband SJ and McVeigh ER. A modified quadropole gradient set for use in high resolution MRI tagging. *Magn Reson Med*, 1994; 32: 246–250.
26. Fischer SE, McKinnon GC, Maier SE and Boesiger P. Improved myocardial tagging contrast. *Magn Reson Med*, 1993; 30:191–200.
27. Rogers WJ, Shapiro EP, Weiss JL, Buchalter MB, Rademakers FE, Weisfeldt ML and Zerhouni EA. Quantification of and correction for left ventricular long-axis shortening by magnetic resonance tissue tagging and slice isolation. *Circulation*, 1991; 84:721–731.
28. Moore CC, O'Dell WG, McVeigh ER and Zerhouni EA. Calculation of three dimensional left ventricular strains from biplanar tagged MR images. *J Magn Reson Imag*, 1992; 2:165–175.
29. O'Dell WG, Moore CC, Hunter WC, Zerhouni EA and McVeigh ER. Three-dimensional myocardial deformations: calculation with displacement field fitting to tagged MR images. *Radiology*, 1995; 195:829–835.
30. Bazille A, Guttman MA, McVeigh ER and Zerhouni EA. Impact of semiautomated versus manual image segmentation errors on myocardial strain calculation by magnetic resonance tagging. *Invest Radiol*, 1994; 29:427–433.
31. Amini AA, Shi P, Constable RT, Johnson K, Duncan J and Gore JC. Energy-minimizing deformable grids for tracking tagged MR cardiac images. *IEEE Proc Comp Cardiol*, 1992; 651–654.
32. Kramer CM, Ferrari VA, Rogers WJ, et al. Angiotensin-

converting enzyme inhibition limits dysfunction in adjacent noninfarcted regions during left ventricular remodeling. *J Am Coll Cardiol*, 1996; 27:211–21.

33. Sayad DE, Willett DL, Hundley WG, Grayburn PA and Peshock RM. Dobutamine magnetic resonance imaging with myocardial tagging quantitatively predicts improvement in regional function after revascularization. *Am J Cardiol*, 1998; 82:1149–1151.
34. Lorenz CH, Fischer SE, Henson RE, Allen JS and Wickline SA. Ventricular torsion in the rat after infarction measured with a whole-body 1.5T MRI scanner. *Ann Biomed Eng*, 1997; 25(Suppl):S65.
35. Young AA, Kramer CM, Ferrari VA, Axel L and Reichek N. Three-dimensional left ventricular deformation in hypertrophic cardiomyopathy. *Circulation*, 1994; 90:854–867.
36. Pastorek JS, Lorenz CH, Bundy JM and Graham TP Jr. Measurement of systolic torsion by MRI differentiates normal myocardium from hypertrophic cardiomyopathy. *J Am Coll Cardiol*, 1996; 27(Suppl):119.
37. Stuber M, Nagel E, Fischer SE, Steinemann F and Boesiger P. Assessment of systolic and diastolic ventricular torsion in pathologic and physiologic hypertrophied hearts [abstract]. Proceedings of the 4th Scientific Meeting of the International Society of Magnetic Resonance in Medicine, New York, April 27 to May 3, 1996, p. 147.
38. Maier SE, Fischer SE, McKinnon GC, Hess OM, Krayenbuehl HP and Boesiger P. Evaluation of left ventricular segmental wall motion in hypertrophic cardiomyopathy with myocardial tagging. *Circulation*, 1992; 86:1919–1928.
39. Yun KL, Niczyporuk MA, Daughters GT, et al. Alterations in left ventricular diastolic twist mechanics during human cardiac allograft rejection. *Circulation*, 1991; 83: 962–973.
40. Buchalter MB, Rademakers FE, Weiss JL, Rogers WJ, Weisfeldt ML and Shapiro EP. Rotational deformation of the canine left ventricle measured by magnetic resonance tagging: effects of catecholamines, ischaemia, and pacing. *Cardiovas Res*, 1994; 28:629–635.
41. Beyar R and Sideman S. The dynamic twisting of the left ventricle: a computer study. *Ann Biomed Eng*, 1986; 14: 547–562.
42. MacGowan G, Burkhoff D, Rogers WJ, Salvador D, Azhari H, Hees PS, Zweier JL, Halperin HR, Siu CO, Lima JA, Weiss JL and Shapiro EP. Effects of afterload on regional left ventricular torsion. *Cardiovas Res*, 1996; 31: 917–925.